One-quasiparticle states in the nuclear energy density functional theory

N. Schunck,[1,2,*] J. Dobaczewski,[3,4,5] J. McDonnell,[1,2] J. Moré,[6] W. Nazarewicz,[1,2,3] J. Sarich,[6] and M. V. Stoitsov[1,2,7]

[1]*Department of Physics and Astronomy, University of Tennessee, Knoxville, Tennessee 37996, USA*
[2]*Physics Division, Oak Ridge National Laboratory, Post Office Box 2008, Oak Ridge, Tennessee 37831, USA*
[3]*Institute of Theoretical Physics, Warsaw University, ul. Hoża 69, PL-00681, Warsaw, Poland*
[4]*Department of Physics, University of Jyväskylä, Post Office Box 35 (YFL), FI-40014, Jyväskylä, Finland*
[5]*Joint Institute for Heavy Ion Research, Oak Ridge National Laboratory, Post Office Box 2008, Oak Ridge, Tennessee 37831, USA*
[6]*Mathematics and Computer Science Division, Argonne National Laboratory, Argonne, Illinois 60439-4844, USA*
[7]*Institute of Nuclear Research and Nuclear Energy, Bulgarian Academy of Sciences, Sofia, Bulgaria*

We study one-quasiproton excitations in the rare-earth region in the framework of the nuclear density functional theory in the Skyrme-Hartree-Fock-Bogoliubov variant. The blocking prescription is implemented exactly, with the time-odd mean field fully taken into account. The equal filling approximation is compared with the exact blocking procedure. We show that both procedures are strictly equivalent when the time-odd channel is neglected and discuss how nuclear alignment properties affect the time-odd fields. The impact of time-odd fields on calculated one-quasiproton band-head energies is found to be rather small, of the order of 100–200 keV; hence, the equal filling approximation is sufficiently precise for most practical applications. The triaxial polarization of the core induced by the odd particle is studied. We also briefly discuss the occurrence of finite-size spin instabilities that are present in calculations for odd-mass nuclei when certain Skyrme functionals are employed.

I. INTRODUCTION

The nuclear density functional theory (DFT) [1–3] plays a central role in the quest for a microscopic and quantitative description of atomic nuclei. The energy functionals related to effective two-body density-dependent interactions are the main building blocks of the mean-field theory of the nucleus wherein the self-consistency is imposed through the Hartree-Fock-Bogoliubov (HFB) formalism. This framework has provided a consistent description of a broad range of phenomena, ranging from nuclear masses to collective excitations. Over the last few years, however, with the influx of high-quality experimental data on exotic nuclei, it has become evident that the standard local functionals (e.g., extended Skyrme functionals) are too restrictive when one is aiming at detailed quantitative description and extrapolability [4–7]. Consequently, various strategies have been devised to develop realistic nuclear energy density functionals (EDFs) [8]. These include (i) using the density matrix expansion technique [9,10] to relate the functional to low-momentum interactions; (ii) extending EDFs by adding higher-order terms in the local densities [11]; and (iii) improving spin and isospin properties [12–15]. In any case, regardless of the strategy, the fine-tuning of the coupling constants of the functional to a suitably chosen set of experimental data is necessary to provide quality description [16].

When aiming at spectroscopic-quality functionals [6], the data coming from odd-mass nuclei are crucial: the energies, angular momenta, and parities of one-quasiparticle (q.p.) excitations provide us with basic knowledge about the underlying shell structure. Moreover, binding energies of odd-*A*

systems are instrumental for determining the magnitude of collective effects such as pairing. Theoretically, however, because nuclei with an odd number of particles have nonzero angular momentum ($J > 0$), that is, they are spin-polarized, their treatment is considerably more involved compared to the $J^\pi = 0^+$ ground-state configurations of doubly even nuclei.

Mathematically, the local EDF is a time-even scalar constructed from various local densities and currents related to particle and pairing density distributions [17,18]. The resulting mean field contains both time-even and time-odd terms. While the time-odd fields automatically vanish in the ground state of doubly even nuclei, they are nonzero in $J > 0$ configurations in which time-reversal symmetry is internally broken [2,3]. Time-odd fields have been investigated in the context of high-spin states [19–22], Gamow-Teller excitations [23], single-particle (s.p.) spectra [6,13,24], and collective dynamics [25–28]. The general consensus is that they can appreciably impact the nuclear collective motion. Nevertheless, our knowledge of the coupling constants characterizing individual time-odd fields is fairly limited, and the impact of those terms on nuclear ground states still needs to be assessed. Conversely, one can ask whether experimental data on nuclear ground states can help constrain the time-odd fields of the nuclear EDF.

There have been very few systematic theoretical studies of one-q.p. states along isotopic or isotonic chains. Regional systematics of one-q.p. excitations, and their consequences on various observables in spherical and deformed nuclei, are given in, for example, Refs. [29–33] (macroscopic-microscopic approach) and Refs. [13,24], and [34–37] (nuclear DFT). The only global DFT study of ground state spin and parity for odd-mass nuclei is that by Bonneau *et al.* [38]. It is to be noted, however, that most of these studies were restricted in one way or another, for example, by assuming

---
*schuncknf@ornl.gov

axial symmetry, neglecting the time-odd fields, or doing an approximate treatment of blocking. The results in Refs. [6,7], and [38] clearly indicate that the currently used nuclear density functionals give a rather poor description of s.p. states, so it is imperative to evaluate the magnitude of the effects owing to theoretical limitations and approximations.

The goal of this study is to review the description of odd-mass nuclei in the framework of the nuclear DFT and assess the magnitude of time-odd polarizations through large-scale surveys. We compare various treatments of blocking, associated approximations, and resulting uncertainties. We discuss the choice of the orientation of the alignment vector, which is important for maintaining s.p. characteristics during the blocking procedure. We also assess the impact of the time-odd fields on binding energies of one-q.p. states and estimate the polarization owing to the axial symmetry breaking in certain orbits.

This paper is organized as follows. Section II summarizes the main features of the nuclear Skyrme DFT. We pay special attention to the treatment of odd-mass nuclei through the so-called blocking approximation and the equal filling approximation (EFA). In Sec. III we present the details of the calculations and discuss various optimization techniques that enable large-scale calculations for odd-mass nuclei. The results are presented in Sec. IV. We first compare the EFA approximation with the exact blocking prescription. We estimate the effect of the time-odd fields on one-q.p. states in the rare-earth region and make selected comparisons with experiment. We also comment on the finite-size instabilities related to certain energy functionals that show up when studying polarized systems. Finally, the conclusions are contained in Sec. V.

II. DENSITY FUNCTIONAL THEORY TREATMENT OF ONE-QUASIPARTICLE STATES

The nuclear DFT in a Skyrme variant has been presented in great detail in a number of articles [2,18,39]. In the following we recall only the salient features of the theory that are needed in this study.

A. Representations of the density matrix

The cornerstone of the nuclear DFT is the general one-body density operator $\hat{\rho}$. Two representations of the density matrix are often considered. In the coordinate representation, the s.p. space is spanned by the continuous basis of states $|r\sigma\rangle = |r\rangle \otimes |\sigma\rangle$ [2,40–42]. In the configuration representation, a basis of discrete states $|n\rangle$ is introduced, where n stands for all the s.p. quantum numbers. The choice of one particular representation depends on the context.

If $|\Phi\rangle$ is the many-body state, the nonlocal density matrix in coordinate representation reads

$$\rho(r\sigma, r'\sigma') = \langle\Phi|c_{r'\sigma'}^\dagger c_{r\sigma}|\Phi\rangle, \tag{1}$$

where $c_{r\sigma}^\dagger$ is a fermionic field operator creating a particle at position r with spin projection σ, and $c_{r\sigma}$ is the corresponding annihilation operator. The field operators can be expressed

in terms of the standard fermionic creation and annihilation operators $c_n^\dagger$ and c_n associated with the basis $|n\rangle$ [43,44]:

$$c_{r\sigma}^\dagger = \sum_n \phi_n^*(r\sigma)c_n^\dagger, \tag{2a}$$

$$c_{r\sigma} = \sum_n \phi_n(r\sigma)c_n. \tag{2b}$$

Note that in this expression, $\phi_n(r\sigma)$ and $\phi_n^*(r\sigma)$ are matrix elements of the basis transformation $|r\sigma\rangle \leftrightarrow |n\rangle$: $\phi_n(r\sigma) = \langle r\sigma|n\rangle$ and $\phi_n^*(r\sigma) = \langle n|r\sigma\rangle$. They are therefore complex s.p. wave functions dependent on the position vector r and spin coordinate σ. The inverse relations are

$$c_n^\dagger = \int d^3r \sum_\sigma \phi_n(r\sigma)c_{r\sigma}^\dagger, \tag{3a}$$

$$c_n = \int d^3r \sum_\sigma \phi_n^*(r\sigma)c_{r\sigma}. \tag{3b}$$

For complete bases, relations (2a), (2b), (3a), and (3b) allow us to express the relations between the two representations, $\rho(r\sigma, r'\sigma')$ and ρ_{mn}, of the density matrix.

The density matrix, Eq. (1), can be regarded as the matrix element of an operator $\hat{\rho}(r\sigma, r'\sigma')$ acting in the spin space. Any such operator can be expressed in terms of the Pauli matrices σ and the identity matrix. This leads to a spin-scalar $\hat{\rho}(r, r')$ and a spin-vector field $\hat{s}(r, r')$. These two fields are the fundamental building blocks of the nuclear DFT.

B. Skyrme energy functional

The contribution to the total energy of the system coming from the Skyrme interaction reads

$$E^{\text{Skyrme}} = \sum_{t=0,1} \int d^3r \{\mathcal{H}_t^{(\text{even})}(r) + \mathcal{H}_t^{(\text{odd})}(r)\}, \tag{4}$$

where $t = 0$ and $t = 1$ correspond to isoscalar and isovector components, respectively. In this article, we do not consider proton-neutron mixing [18]. Using the standard notation for the local densities and currents [17,18], the part of the energy density that depends on time-even fields can be written as

$$\mathcal{H}_t^{(\text{even})}(r) = C_t^\rho \rho_t^2 + C_t^{\Delta\rho}\rho_t\Delta\rho_t + C_t^\tau\rho_t\tau_t + C_t^J \overset{\leftrightarrow}{J}_t^2 + C_t^{\nabla J}\rho_t\nabla \cdot J_t, \tag{5}$$

while the part depending on time-odd fields is

$$\mathcal{H}_t^{(\text{odd})}(r) = C_t^s s_t^2 + C_t^{\Delta s}s_t \cdot \Delta s_t + C_t^T s_t \cdot T_t + C_t^j j_t^2 + C_t^{\nabla j}s_t \cdot (\nabla \wedge j_t). + C_t^F s_t \cdot F_t, \tag{6}$$

All densities and currents entering Eqs. (5) and (6) can be related to the particle density $\rho(r, r')$, the spin density $s(r, r')$, and their derivatives [17,18]. In the present work, we do not consider tensor interactions and therefore we set $C_t^F = 0$.

Here, we discuss several versions of the functional, depending on how the time-odd coupling constants are determined.

   (i) Native version, which corresponds to all time-odd coupling constants being determined by the underlying Skyrme interaction [18].

(ii) Gauge version, which corresponds to the subset of time-odd coupling constants being determined through the gauge-invariance conditions [18,21], namely, $C_t^j = -C_t^\tau$, $C_t^T = -C_t^J$, and $C_t^{\nabla j} = C_t^{\nabla J}$, with all other time-odd coupling constants set to zero.

(iii) Landau version, which is based on the gauge version, where the subset of time-odd coupling constants C_t^s and C_t^T is reset through the Landau parameters [23]:

$$g_0 = N_0\big(2C_0^s + 2C_0^T \beta \rho_0^{2/3}\big),$$
$$g_1 = -2N_0 C_0^T \beta \rho_0^{2/3},$$
$$g_0' = N_0\big(2C_1^s + 2C_1^T \beta \rho_0^{2/3}\big),$$
$$g_1' = -2N_0 C_1^T \beta \rho_0^{2/3}, \tag{7}$$

where $\beta = (3\pi^2/2)^{2/3}$, $1/N_0 = \pi^2 \hbar^2/2m^\star k_F$, and, additionally, $C_t^{\Delta s} = 0$ for $t = 0, 1$. Because the Landau prescription only sets C_t^T, the gauge condition is broken because $C_t^T \neq -C_t^J$ anymore.

(iv) Time-even version, in which all time-odd coupling constants in Eq. (6) are set equal to zero.

C. Hartree-Fock-Bogoliubov method

In the HFB theory, pairing correlations enter through the pairing tensor κ, defined in coordinate representation as

$$\kappa(\boldsymbol{r}\sigma, \boldsymbol{r}'\sigma') = \langle \Phi | c_{\boldsymbol{r}'\sigma'} c_{\boldsymbol{r}\sigma} | \Phi \rangle. \tag{8}$$

(From a practical point of view, it is sometimes more advantageous to use the pairing density $\tilde{\rho}$ [41,42].)

The starting point of the HFB theory is to assume that the ground state of an even-even nucleus is a vacuum for q.p.'s $(\beta_\nu, \beta_\nu^\dagger)$. The latter are obtained from s.p. operators $(c_n, c_n^\dagger)$ associated with the s.p. basis states $|n\rangle$ by the Bogoliubov transformation:

$$\beta_\nu = \sum_n U_{n\nu}^* c_n + V_{n\nu}^* c_n^\dagger, \tag{9a}$$

$$\beta_\nu^\dagger = \sum_n V_{n\nu} c_n + U_{n\nu} c_n^\dagger. \tag{9b}$$

Matrices U and V are obtained from the HFB equations:

$$\begin{pmatrix} \hat{h} - \lambda & \hat{\Delta} \\ -\hat{\Delta}^* & -\hat{h}^* + \lambda \end{pmatrix} \begin{pmatrix} U \\ V \end{pmatrix} = E \begin{pmatrix} U \\ V \end{pmatrix}, \tag{10}$$

where λ is the chemical potential, $\hat{h}$ is Hartree-Fock (HF) potential, and $\hat{\Delta}$ the pairing potential. (From a practical point of view, it is sometimes more advantageous to use the pairing potential $\hat{\tilde{h}}$ [41,42].) The form of the HFB equations in coordinate space is given in Refs. [41] and [42].

The density matrix and pairing tensor can be written as

$$\rho_{mn} = (V^* V^T)_{mn}, \tag{11a}$$

$$\kappa_{mn} = (V^* U^T)_{mn}. \tag{11b}$$

The coordinate representation of the Bogoliubov transformation,

$$\beta_\nu = \int d^3 \boldsymbol{r} \sum_\sigma \big\{ U^{(\nu)*}(\boldsymbol{r}\sigma) c_{\boldsymbol{r}\sigma} + V^{(\nu)*}(\boldsymbol{r}\sigma) c_{\boldsymbol{r}\sigma}^\dagger \big\}, \tag{12a}$$

$$\beta_\nu^\dagger = \int d^3 \boldsymbol{r} \sum_\sigma \big\{ V^{(\nu)}(\boldsymbol{r}\sigma) c_{\boldsymbol{r}\sigma} + U^{(\nu)}(\boldsymbol{r}\sigma) c_{\boldsymbol{r}\sigma}^\dagger \big\}, \tag{12b}$$

can be expressed through lower and upper components of the q.p. wave functions:

$$V^{(\nu)}(\boldsymbol{r}\sigma) = \sum_n \phi_n^*(\boldsymbol{r}\sigma) V_{n\nu}, \tag{13a}$$

$$U^{(\nu)}(\boldsymbol{r}\sigma) = \sum_n \phi_n(\boldsymbol{r}\sigma) U_{n\nu}. \tag{13b}$$

Finally, the density matrix and pairing tensor in coordinate space are

$$\rho(\boldsymbol{r}\sigma, \boldsymbol{r}'\sigma') = \sum_{0 \leqslant E_\mu \leqslant E_{\max}} V^{(\mu)*}(\boldsymbol{r}\sigma) V^{(\mu)}(\boldsymbol{r}'\sigma'), \tag{14a}$$

$$\kappa(\boldsymbol{r}\sigma, \boldsymbol{r}'\sigma') = \sum_{0 \leqslant E_\mu \leqslant E_{\max}} V^{(\mu)*}(\boldsymbol{r}\sigma) U^{(\mu)}(\boldsymbol{r}'\sigma'). \tag{14b}$$

It is assumed that the continuum of q.p. with $E > -\lambda$ has been discretized and all q.p. states with energy lower than some cutoff energy E_{cut} are retained (see discussion in Ref. [41]).

D. The blocking prescription and the equal filling approximation

In the HFB theory, the ground state of an odd nucleus is a one-q.p. excitation, $\beta_{\mu_0}^\dagger$, with respect to the q.p. vacuum. In the configuration representation, the corresponding density matrix and pairing tensor are [45–48]

$$\rho_{mn}^{B,\mu_0} = (V^* V^T)_{mn} + U_{m\mu_0} U_{n\mu_0}^* - V_{m\mu_0}^* V_{n\mu_0}, \tag{15a}$$

$$\kappa_{mn}^{B,\mu_0} = (V^* U^T)_{mn} + U_{m\mu_0} V_{n\mu_0}^* - V_{m\mu_0}^* U_{n\mu_0}. \tag{15b}$$

In practice, one must adopt a prescription to be able to determine, at each iteration, the index μ_0 of the q.p. state to be blocked [49]. In the present study, this has been done according to the recipe described in Ref. [50]. In the first step, the mean-field Hamiltonian $\hat{h}$ is diagonalized:

$$\hat{h} \varphi_n = e_n \varphi_n. \tag{16}$$

Because in this work parity and y signature are assumed to be self-consistent symmetries, every s.p. level e_n is uniquely identified by its position in a given parity and y-signature block. This unique identification allows us to pin down the configuration of the blocking candidate n_0. To connect the s.p. state φ_{n_0} with a q.p. state to be blocked, we calculate at each iteration the overlap between φ_{n_0} and both the upper component U_μ and the time-reversed lower component $V_{\bar{\mu}}$ of q.p. states around the Fermi level [50]. The largest overlap in this set defines the index μ_0 of the q.p. state to be blocked. In the beginning of the iterative process, s.p. states of a neighboring even-even nucleus are taken.

Within the EFA, the state μ_0 and its time-reversal partner $\bar{\mu}_0$ enter the density matrix and pairing tensor with the same

weights, which ensures time-reversal symmetry and, thereby, degeneracy of μ_0 and $\bar{\mu}_0$ [48]:

$$\rho_{mn}^{\mathrm{EFA},\mu_0} = (V^*V^T)_{mn} + \tfrac{1}{2}(U_{m\mu_0}U_{n\mu_0}^* - V_{m\mu_0}^*V_{n\mu_0} \\ + U_{m\bar{\mu}_0}U_{n\bar{\mu}_0}^* - V_{m\bar{\mu}_0}^*V_{n\bar{\mu}_0}), \tag{17a}$$

$$\kappa_{mn}^{\mathrm{EFA},\mu_0} = (V^*U^T)_{mn} + \tfrac{1}{2}(U_{m\mu_0}V_{n\mu_0}^* - V_{m\mu_0}^*U_{n\mu_0} \\ + U_{m\bar{\mu}_0}V_{n\bar{\mu}_0}^* - V_{m\bar{\mu}_0}^*U_{n\bar{\mu}_0}). \tag{17b}$$

The HFB equations are then solved by replacing $(\rho^{B,\mu_0}, \kappa^{B,\mu_0})$ with $(\rho^{\mathrm{EFA},\mu_0}, \kappa^{\mathrm{EFA},\mu_0})$. For the justification of the EFA ansatz by means of statistical density operators and for detailed discussion of the procedure involved, we refer the reader to Refs. [48] and [51].

In this work we point to another possible justification of the EFA. We first note that the time-even parts of the blocked density matrices given by Eqs. (15a) and (15b) are identical to the time-even parts of the density matrices in the EFA, Eqs. (17a) and (17b). Therefore, all time-even densities in Eq. (5) are exactly the same in both variants. Consequently, in the blocking and EFA approximations, the time-even part of the functional (Sec. II B) yields exactly the same self-consistent solution. This allows us to reinterpret EFA density matrices as those corresponding to the time-even functional in which the time-odd polarizations exerted by the odd particle are dynamically switched off. Of course, the blocking prescription and EFA give exactly the same average values of all time-even observables (e.g., radii and multipole moments) but they differ in the average values of time-odd observables (e.g., spin alignments and magnetic moments).

E. Blocking, alignments, and symmetries

Although for the functionals restricted to time-even fields (or within the EFA), the time-reversed q.p states $|\mu\rangle = \beta_\mu^\dagger|0\rangle$ and $|\bar{\mu}\rangle = \beta_{\bar{\mu}}^\dagger|0\rangle$ are exactly degenerate, this is not true any longer in the general case. Here, the blocking prescription does depend on which of these two states, or which linear combination thereof, is used in Eqs. (15a) and (15b). To discuss this point, we introduce here the notion of an "alispin," which pertains to the unitary mixing of states $|\mu\rangle$ and $|\bar{\mu}\rangle$. This is in complete analogy with the standard notion of the isospin, which involves the unitary mixing of proton and neutron states.

An alivector $\mathcal{V}^{(\mu)}$ is defined as a set of two complex numbers, a and b ($|a|^2 + |b|^2 = 1$):

$$\mathcal{V}^{(\mu)} = \begin{pmatrix} a \\ b \end{pmatrix}, \tag{18}$$

which corresponds to the linear combination of states $|\mu\rangle$ and $|\bar{\mu}\rangle$: $|v_\mu\rangle = a|\mu\rangle + b|\bar{\mu}\rangle$. Alivectors reside in SU(2) space; therefore the alirotation by an angle $\boldsymbol{\phi}^{(\mu)}$ is defined as

$$\mathcal{V}^{(\mu)'} = \begin{pmatrix} a' \\ b' \end{pmatrix} = e^{i\boldsymbol{\phi}^{(\mu)} \circ \boldsymbol{\sigma}^{(\mu)}} \begin{pmatrix} a \\ b \end{pmatrix}, \tag{19}$$

where the alivectors of Pauli matrices are denoted $\boldsymbol{\sigma}^{(\mu)}$, and $\circ$ denotes the scalar product of alivectors. To recall that the alirotation pertains to a single pair of states, we use the superscript (μ) throughout.

The blocked density matrix, Eq. (15a), corresponding to the state $\mathcal{V}^{(\mu)}$ reads

$$\rho_{mn}^{B,(a,b)} = \rho_{mn} - \{|a|^2 V_{n\mu}V_{m\mu}^* + |b|^2 V_{n\bar{\mu}}V_{m\bar{\mu}}^* + a^*b V_{n\bar{\mu}}V_{m\mu}^* \\ + ab^* V_{n\mu}V_{m\bar{\mu}}^*\} + \{|a|^2 U_{n\mu}^*U_{m\mu} + |b|^2 U_{n\bar{\mu}}^*U_{m\bar{\mu}} \\ + a^*b U_{n\bar{\mu}}^*U_{m\mu} + ab^* U_{n\mu}^*U_{m\bar{\mu}}\}. \tag{20}$$

If time-reversal symmetry is conserved, the different blocks of the Bogoliubov matrices are related:

$$-V_{\bar{n}\mu}^* = V_{n\bar{\mu}} \quad \text{and} \quad V_{n\mu}^* = V_{\bar{n}\bar{\mu}}, \tag{21}$$

and $\rho_{mn}^{(a,b)} = \rho_{\bar{m}\bar{n}}^{(a,b)*}$. These relations lead to

$$\rho_{mn}^{(ab)} = \rho_{mn} - V_{n\mu}V_{m\mu}^* + U_{n\mu}^*U_{m\mu} \tag{22}$$

or, equivalently,

$$\rho_{mn}^{(ab)} = \rho_{mn} - V_{n\bar{\mu}}V_{m\bar{\mu}}^* + U_{n\bar{\mu}}^*U_{m\bar{\mu}}. \tag{23}$$

Therefore, in this limit, the exact blocking density matrix becomes independent of the coefficients (a, b) of the mixing, that is, it is an aliscalar. Because

$$\rho_{mn}^{\mathrm{EFA}} = \tfrac{1}{2}\left(\rho_{mn}^{(1,0)} + \rho_{mn}^{(0,1)}\right), \tag{24}$$

the EFA density matrix also coincides with the exact blocking density matrix; hence, it is an aliscalar as well.

In the general case where time-reversal symmetry is not dynamically conserved, however, the blocking density matrix is not aliscalar and the energy of the system may change as a function of the mixing coefficients (a, b). To analyze the consequences of blocking different alirotated states $\mathcal{V}^{(\mu_0)'}$, we introduce the (real) alignment vector $\boldsymbol{J}^{(\mu)} = \langle\mu|\hat{\boldsymbol{J}}|\mu\rangle = -\langle\bar{\mu}|\hat{\boldsymbol{J}}|\bar{\mu}\rangle$ and the (complex) decoupling vector $\boldsymbol{D}^{(\mu)} = \langle\mu|\hat{\boldsymbol{J}}|\bar{\mu}\rangle = \langle\bar{\mu}|\hat{\boldsymbol{J}}|\mu\rangle^*$ [52]. Together, they form the matrix elements of the alignment vector-alivector $\hat{\mathcal{J}}^{(\mu)}$:

$$\hat{\mathcal{J}}^{(\mu)} = \begin{pmatrix} \boldsymbol{J}^{(\mu)} & \boldsymbol{D}^{(\mu)} \\ \boldsymbol{D}^{(\mu)*} & -\boldsymbol{J}^{(\mu)} \end{pmatrix}. \tag{25}$$

Expanding this operator [acting on SU(2) alistates] in the basis of Pauli matrices, we find

$$\hat{\mathcal{J}}_1^\mu = +\Re\boldsymbol{D}^\mu, \tag{26a}$$

$$\hat{\mathcal{J}}_2^\mu = -\Im\boldsymbol{D}^\mu, \tag{26b}$$

$$\hat{\mathcal{J}}_3^\mu = +\boldsymbol{J}^\mu, \tag{26c}$$

where indices $k = 1, 2, 3$ enumerate the components of alivectors. From these considerations it follows that the alignment vector-alivector $\hat{\mathcal{J}}^{\mu'}$, which corresponds to the alirotated pair, Eq. (19), is obtained by

$$\begin{pmatrix} \hat{\mathcal{J}}_1^{\mu'} \\ \hat{\mathcal{J}}_2^{\mu'} \\ \hat{\mathcal{J}}_3^{\mu'} \end{pmatrix} = \exp(i\vec{\phi}_\mu \circ \vec{S}_\mu) \begin{pmatrix} \hat{\mathcal{J}}_1^\mu \\ \hat{\mathcal{J}}_2^\mu \\ \hat{\mathcal{J}}_3^\mu \end{pmatrix}, \tag{27}$$

where $\vec{S}_\mu$ are the standard spin-1 matrices [53], which are generators of rotation in the vector representation. This shows that the concept of alirotation (equivalent to changing the mixing of the blocked state) translates into a change in the alignment of the system.

To illustrate how this works, let us examine the special case where the states $|\mu\rangle \equiv |\mu_y\rangle$ and $|\bar{\mu}\rangle \equiv |\bar{\mu}_y\rangle$ are eigenstates of the $\hat{R}_y$ signature operator. Because

$$\hat{R}_i \hat{R}_j = \sum_k \varepsilon_{ijk} \hat{R}_k, \qquad (28)$$

we can express the states $|\mu_y\rangle$ and $|\bar{\mu}_y\rangle$ in terms of $\hat{R}_z$ eigenstates:

$$\begin{pmatrix} |\mu_y\rangle \\ |\bar{\mu}_y\rangle \end{pmatrix} = \begin{pmatrix} +\dfrac{1}{\sqrt{2}} e^{-i\pi/4} & +\dfrac{1}{\sqrt{2}} e^{-i\pi/4} \\ -\dfrac{1}{\sqrt{2}} e^{+i\pi/4} & +\dfrac{1}{\sqrt{2}} e^{+i\pi/4} \end{pmatrix} \begin{pmatrix} |\mu_z\rangle \\ |\bar{\mu}_z\rangle \end{pmatrix}, \quad (29)$$

which corresponds to the rotation of the system by the Euler angles $(\alpha, \beta, \gamma) = (0, \pi/2, \pi/2)$. Consequently, the alivector $\mathcal{V}^{(\mu_y)}$ is the vector $\mathcal{V}^{(\mu_z)}$ alirotated by the angles $\boldsymbol{\phi}^{(\mu)} = (\alpha, \beta, \gamma)$. Because (i) the blocked density matrix is not an aliscalar, and (ii) alirotations are induced by rotations of the coordinate system or, equivalently, a change of the symmetry operators used to label s.p. and q.p. states, we must conclude that the blocked density matrix may depend on the choice of the symmetry operators that commute with the Hamiltonian.[1]

More generally, as all alignment properties of the system are embedded in the vector-alivector operator $\hat{\mathcal{J}}$, we also see that the alirotation of states $|\mu\rangle$ and $|\bar{\mu}\rangle$ corresponds to HFB states having different alignment vectors. Therefore, the latter can be used to tag blocked states. This is a very convenient method, which can be applied not only in the time-even version of the functional when the q.p. states $|\mu\rangle$ and $|\bar{\mu}\rangle$ are degenerate, but also in the case of internally broken time-reversal symmetry. The key to our considerations of blocked states is the realization that blocking must depend on the orientation of the alignment vector with respect to the principal axes of the mass distribution. Therefore, the only rigorous way to proceed would be for each q.p. excitation to vary the orientation of the alignment vector with respect to the principal axes of the system and retain the solution with the lowest energy [54]. We give a pedagogical illustration of such anisotropy of blocking in Sec. IV B 3.

In many practical applications, however, one chooses a fixed direction of alignment dictated by practical considerations. In particular, the identification of blocked s.p. states n and q.p. states μ_0 is most conveniently carried out through the set of conserved quantum numbers characteristic of the problem. In all calculations performed in this work, nuclei are either axially deformed or nearly axial, and they conserve reflection symmetry. The corresponding symmetry group is D_{2h}^{TD}; hence, signature $r = \pm i$ and parity $\pi = \pm 1$ are good quantum numbers. In HFODD the signature is defined with respect to the

---

[1]Note that, in the particular case where the alivector is built from the eigenstates $|\mu_y\rangle$ and $|\bar{\mu}_y\rangle$ of $\hat{R}_y$, the alirotation by $(0, \pi, 0)$ is equivalent to the $\hat{R}_y$ symmetry and therefore, leaves the system invariant. This operation corresponds to $(|\mu_y\rangle, |\bar{\mu}_y\rangle) \rightarrow (+|\bar{\mu}_y\rangle, -|\mu_y\rangle)$. Therefore, in this particular case, blocking state $|\mu_y\rangle$ or state $|\bar{\mu}_y\rangle$ gives exactly the same energy, even though time-reversal symmetry is internally broken and the q.p. spectra do not exhibit the Kramers degeneracy.

y axis of the reference frame [55]. In this way, the alignment vector is restricted to having only the y component. To realize the three possible alignments of the angular momentum along the principal axes, it is sufficient to orient the longest, shortest, or intermediate axis along the y axis. Because in most cases, the configurations analyzed in this study are axial, only two orientations suffice. We show in Sec. III A how to implement such a scenario.

Equivalently, one could work with a good z-simplex basis such as in Ref. [56]. In that case, the default alignment is along the z axis, but the results still depend on the orientation of the body. Only if the alignment vector were allowed to cover the full solid angle would the physical properties of the system not depend on the choice of the basis used to describe the odd nucleus.

III. METHOD OF CALCULATION AND OPTIMIZATION TECHNIQUES

This section briefly describes the DFT solvers used in this work and discusses the choice of parameters entering our calculations. We also outline various optimization techniques that we have implemented to carry out large-scale DFT calculations for one-q.p. states on leadership-class computers.

A. Numerical parameters

All calculations in this work are performed with the DFT solvers HFBTHO [57] and HFODD [50,55,58]. Both codes solve the Skyrme HFB problem in the configuration space by means of the harmonic oscillator (HO) expansion technique. In HFBTHO, the cylindrical HO basis is used, and both axial and time-reversal symmetries are imposed. This implies that the EFA must be used for blocking calculations. The three-dimensional solver HFODD employs the Cartesian HO basis and is symmetry unrestricted. This unique feature of HFODD makes it a tool of choice for our study, as in the polarized nuclear configurations many self-consistent symmetries are usually broken. The blocking prescription is implemented exactly in HFODD with all the time-odd fields taken into account. The two codes have been benchmarked against one another and they yield the same results within a few electronvolts for spherical or axially deformed even-even nuclei [59].

As already mentioned, all nuclei considered in this work are either axial or slightly triaxial, as well as reflection symmetric. Therefore the y signature and parity are conserved and used in HFODD to tag q.p. and s.p. states. However, this implies that the total alignment is confined to the y axis. Because the latter is not the quantization axis, one cannot easily associate the s.p. spin Ω with the expectation value of the angular momentum: the situation is analogous to the collective rotation in high-spin physics. For the sake of identification of deformed Nilsson orbitals, it is convenient, however, to reintroduce Ω as a (nearly) good quantum number by orienting the angular momentum along the z axis; the resulting alignment properties correspond to the limit of noncollective rotation.

To this end, we need to associate the quantization axis with the symmetry axis of the nucleus. This can be achieved via a

Euler rotation of the body-fixed frame (by $\alpha = \pi/2$, $\beta = \pi/2$, $\gamma = 0$) or by imposition of constraints on the expectation values of the quadrupole tensor $\hat{Q}_{2\mu}$. After testing these two options, we choose the Euler rotation: calculations for even-even nuclei are performed in the standard y-signature mode, then solutions are Euler-rotated and used to warm-start calculations for odd nuclei. In this way, the Nilsson quantum number Ω is computed from the expectation value of $\hat{j}_y$. This technique turns out to be both stable and fast. Note that the energies of a given blocked state in the Euler-rotated case and original orientation are different, as discussed in Sec. II E. Only a complete survey of all possible orientations of the alignment vector, which would be a major computational endeavor, could pin down the correct orientation.

As is well known, calculations for deformed nuclei converge faster if the eigenstates are expanded on a stretched basis that follows the geometry of the nuclear density. Unfortunately, the stretched basis is not compatible with the Euler rotation of the nucleus in space in HFODD. For that reason, all calculations presented in this work have been carried out in a full spherical basis of $N_{\rm osc} = 14$ oscillator shells (the number of basis states is $N_s = 680$). This choice guarantees stability of results for the relatively modest deformations considered in this study. The oscillator frequency was fixed at $1.2 \times \hbar\omega_0$ [60] for $\hbar\omega_0 = 41/A^{1/3}$ MeV.

In this work, we use three commonly used Skyrme parametrizations: SIII [61], SkP [41], and SLy4 [62]. In the pairing channel, we employ the density-dependent δ interaction in the mixed variant [63]:

$$V(\boldsymbol{r}, \boldsymbol{r}') = V_0 \left[1 - \frac{1}{2} \frac{\rho(\boldsymbol{r})}{\rho_0} \right] \delta(\boldsymbol{r} - \boldsymbol{r}'), \qquad (30)$$

where $\rho_0 = 0.16$ fm^{-1} and V_0 is the pairing strength (identical for protons and neutrons). Note that the use of such a zero-range interaction requires us to introduce a renormalization (or regularization) procedure to avoid nonphysical divergences [64,65]. We employ the standard value $E_{\rm cut} = 60$ MeV.

For each Skyrme EDF, the pairing strength V_0 has been adjusted to reproduce the experimental proton odd-even mass difference in the deformed nucleus ^{162}Dy, $\Delta_p^{(3)} = 0.60$ MeV. This choice has been motivated by the findings of Ref. [66] that, by adjusting V_0 to experimental data for a spherical semimagic nucleus, one underestimates pairing correlations in deformed systems having a lower s.p. level density around the Fermi surface. Moreover, by considering the proton pairing gap, one effectively takes into account the Coulomb contribution to pairing [67]. The pairing strengths used in this work are $V_0 = -314.406$, -297.303, and -249.059 MeV for SLy4, SIII, and SkP, respectively. In Sec. IV E, we also consider SkO, $V_0 = -269.226$ MeV, and SkM*, $V_0 = -297.875$ MeV.

B. Parallelization and optimization

The advent of Teraflop and Petaflop supercomputers enables large-scale surveys with symmetry-unrestricted DFT solvers. To optimize resources, however, optimization of the production codes is required. Starting from the original published versions of HFODD and HFBTHO, we made a number of improvements. First, a parallel interface using the standard

message passing interface (MPI) has been constructed to allow the automated distribution of calculations over several computing cores. Let us note that the standard nuclear DFT calculations are "embarrassingly parallel." Indeed, solving the HFB equations for one nuclear configuration usually does not take more than a few hours on a standard desktop computer. Therefore, each computing core of a massively parallel system can process a single HFB task corresponding to a particular nucleonic configuration. Only in the limit of very large HO bases, or for DFT solvers constructed in the coordinate space, does the parallelization of the solvers become necessary. The advantage of using massively parallel architectures is that simultaneous calculations of hundreds or thousands of different many-body configurations are possible in a very reasonable time. Such a strategy makes it possible to extract systematic trends, use standard statistical analysis toolboxes, and ultimately develop nuclear EDFs of spectroscopic quality.

The scaling of a DFT problem with the number of processors also implies that a simple master-slave parallel architecture is sufficient for most applications, and this solution is adopted here. All calculations in this study were performed on the Cray XT3/XT4 Jaguar supercomputer at the National Center for Computational Science at the Oak Ridge National Laboratory and on the Cray XT3 Franklin supercomputer at the National Energy Research Scientific Computing Center at the Lawrence Berkeley National Laboratory. Typical production runs have involved from 8000 to 12 000 computing cores per run, and the typical calculation time was about 2 h.

The HFB equations represent a coupled system of nonlinear equations for nucleonic densities. The nonlinearity enters through the dependence of the mean fields on densities (self-consistency). To diminish the number of iterations required to attain a given precision, we employ the modified Broyden method [68,69]. The method is based on the observation that the convergence of the HFB process stops when the characteristic variables in the problem, for example, the density ρ, does not change any more from one iteration to the next: $||\rho^{(n+1)} - \rho^{(n)}|| \approx 0$. In other words, the HFB equations can be viewed as a fixed-point problem, and iterations can therefore be optimized by employing a quasi-Newton method. It was shown that the computational cost (in units of number of iterations) could be reduced substantially, by a factor of 3 to 4. Our particular implementation of the modified Broyden method is described in Ref. [69].

As mentioned earlier, HFODD solves the HFB problem by expanding eigenvectors in the Cartesian HO basis. In terms of speed, one of the major bottlenecks in HFODD is the diagonalization of the HFB matrix. The latter is carried out with the subroutine ZHEEVR of the LAPACK library. We found that a significant gain in terms of speed, up to 30%–40% for large HO bases with, for example, $N_{\rm osc} = 20$ shells, could be obtained by using machine-specific implementations of the BLAS and LAPACK libraries, such as ATLAS.

C. Massively parallel calculations: Convergence improvements

Based on the experience gained in self-consistent calculations for odd-A nuclei, it appears that calculations involving blocking are always less stable than those performed for

even-even nuclei. Apart from the specific issue related to finite-size instabilities addressed in Sec. IV E, these numerical instabilities are related to the need to select, at each iteration, the blocked q.p. state. The blocking procedure is outlined in Sec. II D and the detailed justification is given in, for example, Ref. [49]. The selection method implies that the blocked q.p. state may change from one iteration to the next, in particular, at the beginning of the calculation. This numerical noise is the price paid for the full self-consistency, and it explains why small differences in the initial conditions can actually affect the convergence process.

When only a few nuclei are considered, and a small number of blocked configurations near the ground state is calculated, one can often find ways to converge calculations, such as (i) changing the linear-mixing parameter of the self-consistent scheme; (ii) starting from the unblocked, fully paired state corresponding to an odd average particle number (false vacuum) [70]; (iii) starting from the even-even nucleus with one more particle for a particle-like blocked state and with one particle less for a holelike blocked state, as implemented in Ref. [49] (we also used this method in our calculation); and (iv) using different values of the linear-mixing parameter for time-even, time-odd, and/or pairing fields. Whenever a blocking calculation fails to converge, one may repeat it by using one or several of these tricks until a converged result is obtained. This is what was done in previous studies involving self-consistent calculations, and it was possible because these studies were focused on ground-state properties and only a minimum number of different configurations was considered.

In our case, however, we consider thousands of configurations, and such a trial-and-error scheme, however helpful, is simply impossible to implement. Instead, we have resorted to a simple trick, namely, as the initial conditions do matter, we artificially generate slightly different initial conditions for the two signature partners that converge to practically the same result.

The main idea here consists in adding a tiny rotational frequency of about $\hbar\omega = 0.001$ MeV to break the degeneracy of signature configurations. This improves the convergence rate at the price of an insignificant numerical error of about 1–2 keV, on average. We illustrate this fact by two specific examples of blocked states in ^{163}Tb (native version, noncollective orientation) with different alignments. For the blocked state [411]1/2, at $\hbar\omega = 0$ the total energy equals $-1322.279\ 268$ MeV, while for $\hbar\omega = +0.001$ and -0.001 MeV the total energies read $-1322.279\ 480$ MeV ($J_\parallel = -\Omega = -1/2$) and $-1322.279\ 188$ MeV ($J_\parallel = +\Omega = +1/2$), respectively. Similarly, for the blocked state [404]7/2, the three corresponding energies are $-1321.725\ 322$ MeV, $-1321.725\ 538$ MeV ($J_\parallel = -\Omega = -7/2$), and $-1321.726\ 010$ MeV ($J_\parallel = +\Omega = +7/2$). To make our point, we deliberately show these energies with far more digits than are physically relevant. In these particular two examples, the numerical precision of the calculation is 10 eV, which is exceptionally good for odd nuclei. Therefore, the noted differences can only be attributed to the effect of the cranking term. Without this term, by blocking states μ_0 and $\bar\mu_0$ one always obtains exactly the same HFB energy, $E_{\mu_0} = E_{\bar\mu_0}$, because the full Skyrme functional is time-even.

IV. RESULTS

This section presents a number of Skyrme HFB results for odd-mass nuclei. We begin by giving a detailed numerical comparison of the EFA with the exact blocking prescription in the limit of conserved time-reversal symmetry. The impact of time-odd fields on the q.p. spectrum in the rare-earth region is shown in Sec. IV B, with the native, gauge, and Landau versions of SIII, SkP, and SLy4 functionals. The role of the nuclear alignment vector on physical observables is also studied. Results of calculations are compared with selected experimental data in Sec. IV C. The triaxial polarization induced by a blocked quasiparticle is discussed in Sec. IV D. Finally, Sec. IV E mentions the problem of the intrinsic instability of certain Skyrme functionals that appear when time-odd terms are included.

A. Validation of the equal filling approximation

To demonstrate the numerical precision of our calculations, Table I reports the results for four one-quasineutron states in ^{121}Sn obtained with HFBTHO (EFA) and HFODD (exact blocking). They are selected based on the mean-field spectrum, Eq. (16), of ^{120}Sn. For the sake of this comparison, the time-odd fields in HFODD have been switched off, thereby enforcing the regime where the exact blocking procedure is strictly equivalent to the EFA; see Sec. II D. Indeed, the numerical differences obtained between the EFA and exact blocking are extremely small, less than 1 keV for the four cases reported in Table I. This can be entirely attributed to various implementations adopted differently in the two codes such as the method of computing the Coulomb potential. The even-even core ^{120}Sn is spherical in its ground state. The q.p. blocking slightly polarizes the nuclear shape, inducing small quadrupole deformations for some configurations.

Although the time-even observables obtained within the EFA and exact blocking are strictly identical if the time-odd fields are disregarded, this is not true for time-odd observables. In Table I, this is illustrated by the values of alignments of the blocked q.p.'s aligned parallel ($J_\parallel$) or perpendicular ($J_\perp$) to the symmetry axis. Of course, without time-odd fields, the direction of alignment does not influence the time-even observables.

Rare-earth nuclei provide an excellent testing ground for studies of deformed Nilsson orbits. Many of those nuclei are well-deformed, near-axial rotors and the deformed mean-field theory is particularly suitable to describe their structural properties. Table II reports a comparison for several one-quasiproton configurations in a well-deformed odd-proton nucleus ^{163}Tb. In HFBTHO, the determination of a blocking candidate was made using the mean-field spectrum, Eq. (16), of the even-even core ^{162}Dy. In the case of HFODD, to improve the speed and stability of the iterative process [49], blocking candidates of a particle character (above the proton Fermi level of ^{162}Dy) were selected from the mean-field spectrum of ^{164}Dy, while holelike levels were selected from that of ^{162}Dy. Of course, the final results do not depend on which particular even-even nucleus has been used as a core.

The results reported in Table II show again that, without time-odd fields, the full blocking procedure is equivalent to

TABLE I. Comparison of EFA (HFBTHO) with exact blocking (HFODD) for four one-quasineutron configurations in ^{121}Sn. Time-odd fields are switched off. Quasiparticle energy E_{qp}, neutron chemical potential λ_n, neutron pairing energy E^n_{pair}, average neutron pairing gap $\Delta_n = \mathrm{Tr}(\Delta\rho)/N$, total r.m.s. radius, axial quadrupole deformation β, total quadrupole moment Q_{tot}, kinetic energy E_{kin} (for protons and neutrons), total spin-orbit energy E_{SO}, direct Coulomb energy E_{dir}, and total energy E_{tot} are listed. The last two lines show the HFODD alignments of the blocked quasiparticles: $J_\parallel$ was calculated in the noncollective orientation, and $J_\perp$ in the collective orientation (see discussion in Sec. IV B3). In the EFA total alignments are equal to 0 by construction. Orbits are labeled with the $\ell_j(\Omega^\pi)$ quantum numbers. The SLy4 functional is used in the particle-hole channel and the density-dependent δ interaction with $V_0 = -285.634$ MeV. Differences between HFBTHO and HFODD results are in boldface.

	$d_{3/2}(1/2^+)$		$d_{3/2}(3/2^+)$		$h_{11/2}(5/2^-)$		$g_{7/2}(7/2^+)$	
	EFA	Exact	EFA	Exact	EFA	Exact	EFA	Exact
E_{qp} (MeV)	1.00**76**	1.0080	1.182**2**	1.1820	1.4570	1.4570	2.28**79**	2.2880
λ_n (MeV)	-7.7496	-7.7496	-7.7288	-7.7288	-7.983**4**	-7.9836	-7.6371	-7.6371
E^n_{pair} (MeV)	-9.294**9**	-9.2948	-9.441**1**	-9.4410	-8.714**5**	-8.7147	-10.40**41**	-10.4036
Δ_n (MeV)	1.0575	1.0575	1.0667	1.0667	1.0395	1.0395	1.1206	1.1206
r.m.s (fm)	4.6895	4.6895	4.6889	4.6889	4.6894	4.6894	4.6884	4.6884
β	-0.0257	-0.0257	0.0131	0.0131	0.009**9**	0.0098	0.0340	0.0340
Q_{tot} (b)	-0.862**7**	-0.8624	0.4383	0.4383	0.33**01**	0.3351	1.1409	1.1409
E^n_{kin} (MeV)	1360.438**5**	1360.4384	1360.9970	1360.9970	1358.89**95**	1358.8980	1364.56**96**	1364.5680
E^p_{kin} (MeV)	827.317**6**	827.3177	827.3582	827.3582	827.189**2**	827.1890	828.1830	828.1830
E^{tot}_{SO} (MeV)	-50.4839	-50.4839	-50.8174	-50.8174	-49.58**56**	-49.5844	-54.65**31**	-54.6529
E_{dir} (MeV)	365.7437	365.7437	365.7638	365.7638	365.738**7**	365.7386	365.99**80**	365.9979
E_{tot} (MeV)	-1024.707**4**	-1024.7073	-1024.6538	-1024.6538	-1024.385**6**	-1024.3855	-1023.4465	-1023.4465
$J_\parallel$ ($\hbar$)	0.00	0.50	0.00	1.50	0.00	2.50	0.00	3.50
$J_\perp$ ($\hbar$)	0.00	0.82	0.00	0.00	0.00	0.43	0.00	0.01

the EFA. It is worth noting that the difference in the total energy is less than 1 keV for all of the excited states, and less than 0.002 b for the quadrupole moments, regardless of the quadrupole polarization exerted by a blocked state.

B. Effect of time-odd fields

This section illustrates the effect of the various prescriptions for the time-odd channel, Eq. (6), of the functionals. Calcula-

TABLE II. Comparison of EFA (HFBTHO) with exact blocking (HFODD) for 10 one-quasiproton configurations in ^{163}Tb. Total energy E_{tot} and total quadrupole moment Q_{tot} are listed. Orbits are labeled with the asymptotic Nilsson quantum numbers $[Nn_z\Lambda]\Omega^\pi$. The SIII Skyrme functional is used in the particle-hole channel. Time-odd fields are disregarded. Differences between HFBTHO and HFODD results are in boldface.

Blocked state	EFA (HFBTHO)		Exact (HFODD)	
	Q_{tot} (b)	E_{tot} (MeV)	Q_{tot} (b)	E_{tot} (MeV)
$[411]3/2^+$	18.514	-1323.495	18.514	-1323.495
$[532]5/2^-$	17.759	-1322.64**8**	17.759	-1322.647
$[523]7/2^-$	18.55**4**	-1322.41**5**	18.55**5**	-1322.41**4**
$[411]1/2^+$	18.384	-1322.322	18.384	-1322.322
$[413]5/2^+$	18.654	-1322.151	18.654	-1322.151
$[541]1/2^-$	20.13**8**	-1321.77**1**	20.13**6**	-1321.77**3**
$[541]3/2^-$	17.29**1**	-1321.357	17.29**0**	-1321.357
$[530]1/2^-$	17.034	-1320.762	17.03**2**	-1320.762
$[420]1/2^+$	17.766	-1320.090	17.76**7**	-1320.090
$[404]9/2^+$	19.266	-1319.851	19.266	-1319.851

tions were performed for all odd-proton nuclei with $63 \leqslant Z \leqslant 75$ and $78 \leqslant N \leqslant 104$. For each of them, 14 nondegenerate blocked configurations around the Fermi level have been considered. Altogether, 3822 independent one-quasiproton states were studied.

1. Native functionals

Table III displays results for one-quasiproton states in ^{163}Tb in the time-even, native, gauge, and Landau variants of calculations. The alignment and elongation axes coincide with the y axis of the reference frame. The time-even energies are shown in the absolute scale. For other variants, displacements

TABLE III. Energies (MeV) of one-quasiproton configurations in ^{163}Tb calculated using the time-even, native, gauge, and Landau variants of the SIII Skyrme functional; see Sec. II B. Results for the time-even variant are shown in the absolute scale, while those for the other variants are shown as shifts, Eq. (31).

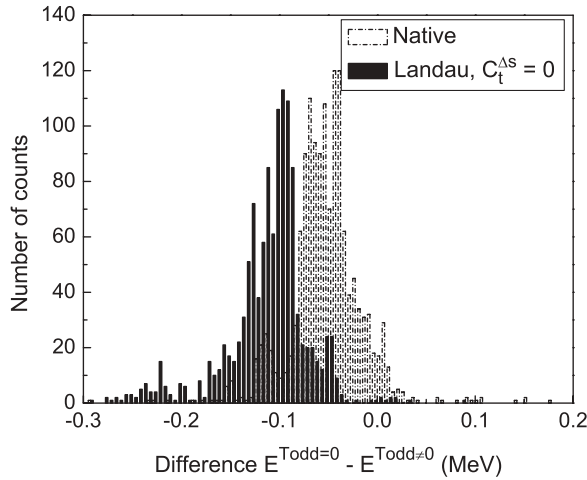| Blocked state	Time even	Native	Gauge	Landau
$[411]3/2^+$	-1323.495	-0.075	$+0.042$	-0.125
$[532]5/2^-$	-1322.647	-0.052	$+0.029$	-0.105
$[523]7/2^-$	-1322.410	-0.060	$+0.039$	-0.080
$[411]1/2^+$	-1322.322	-0.043	$+0.040$	-0.118
$[413]5/2^+$	-1322.151	-0.048	$+0.062$	-0.085
$[541]1/2^-$	-1321.773	-0.007	$+0.055$	-0.075
$[541]3/2^-$	-1321.357	-0.047	$+0.036$	-0.107
$[530]1/2^-$	-1320.762	-0.037	$+0.017$	-0.161
$[420]1/2^+$	-1320.090	-0.127	$+0.018$	-0.231
$[404]9/2^+$	-1319.851	-0.121	$+0.036$	-0.150

FIG. 1. Cumulative histogram of energy differences, Eq. (31), for one-quasiproton states in deformed rare-earth nuclei calculated with SIII, SkP, and SLy4 EDFs. Dot-dashed open bins, native functionals; filled bins, Landau functionals. The bin size is 5 keV.

with respect to the time-even case are shown:

$$\Delta E^{\text{Todd}} = E_{\text{qp}}^{\text{Todd}=0} - E_{\text{qp}}^{\text{Todd}\neq 0}. \tag{31}$$

In the particular example reported in Table III, the maximum shift in one-q.p. levels owing to the time-odd terms of the native functional is 127 keV. This is consistent with the earlier results in Refs. [70] and [71] and overall smaller than in the relativistic mean-field approach, where time-odd polarization corrections seem to range from only a few dozen kiloelectronvolts in deformed actinides up to half a megaelectronvolt in light nuclei [36,37].

The overall impact of the time-odd fields on the energy of one-quasiproton states in the deformed rare-earth nuclei is summarized in Fig. 1, which shows the distribution of ΔE^{Todd} (31) for SIII, SkP, and SLy4 EDFs. When native functionals are used, the total number of converged cases is 1404 (524 for SIII, 443 for SkP, and 437 for SLy4). The average value of ΔE^{Todd} is -50 keV, with a standard deviation of 42 keV.

The magnitude of the time-odd effect depends on the choice of the EDF. To illustrate this point, Fig. 2 displays the distribution of ΔE^{Todd} for individual functionals. Focusing in this section on the native functionals (dot-dashed open bins), it is shown that the largest time-odd effect is predicted for SIII, which also shows an appreciable spread in values (configuration dependent). On the contrary, for the SkP parametrization the distribution of ΔE^{Todd} is fairly narrow, centered around -40 keV.

By construction, Figs. 1 and 2 contain contributions from ground-state configurations and from nearly lying excited states. Because ground-state values are of particular importance, as they impact mass predictions, Fig. 3 shows ΔE^{Todd} for ground-state configurations only. The average value of the ground-state time-odd displacement is only $\sim$50 keV. Most of the few cases with $|\Delta E_{\text{gs}}^{\text{Todd}}| > 150$ keV in fact correspond to a collapse of pairing correlations in one of the two sets of calculations. It may be worth noting that the most recent HFB
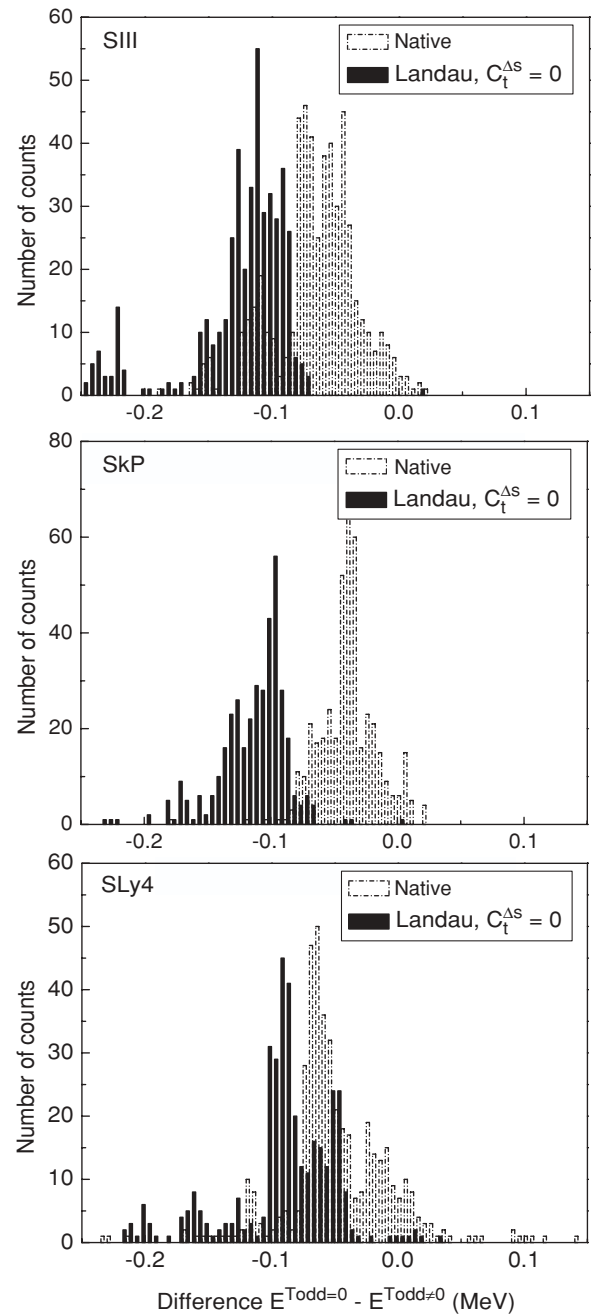

FIG. 2. Similar to Fig. 1 except for individual Skyrme functionals: SIII (top), SkP (middle), and SLy4 (bottom).

mass formula based on the Skyrme BSk17 parametrization yields a root mean square (r.m.s.) deviation of 581 keV [16]. The uncertainty associated with neglecting the time-odd fields appears, therefore, to be smaller by an order of magnitude.

To discuss the configuration dependence of the time-odd displacement, it is instructive to identify the s.p. orbits of interest. To this end, Fig. 4 shows the evolution of the proton s.p. energies, defined as the eigenvalues of the mean-field operator, Eq. (16), in the nucleus ^{164}Dy calculated with SLy4 as a function of the axial quadrupole deformation α_{20}. This Nilsson diagram has been obtained by carrying out a set of
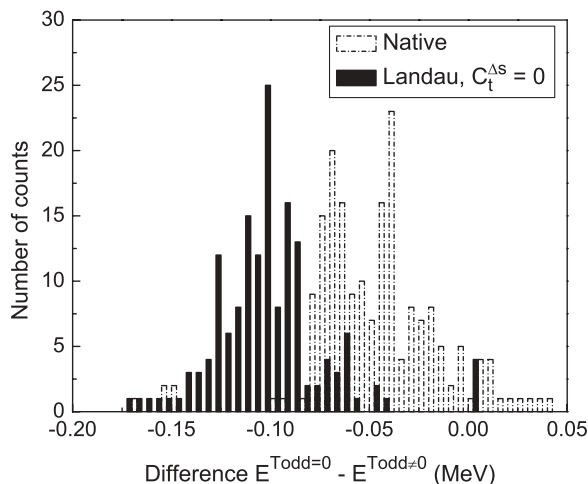
FIG. 3. Similar to Fig. 1 but for ground-state configurations only.

constrained HFB calculations along a one-dimensional $\langle \hat{Q}_{20} \rangle$ path.

Although the values of ΔE^{Todd} are usually small, there are a few cases where the displacement can amount to more than 100 keV. A detailed analysis of the blocked configurations for all three interactions shows that the largest deviations correspond essentially to the [420]1/2, [404]9/2, [400]1/2, and [505]11/2 Nilsson orbitals. It is interesting to note that the value of the s.p. angular momentum does not seem to be crucial, as these states can be associated with both low- and high-j spherical shells. In deformed rare-earth nuclei, equilibrium deformations are $\alpha_{20} \sim 0.25$–0.30. As shown in Fig. 4, in this deformation range, the orbital [420]1/2 is a deep-hole state, while [404]9/2, [400]1/2, and [505]11/2 are highly excited particle states. All these one-quasiproton excitations are strongly oblate driving. A similar result has also been obtained for SLy4 and SkP.

2. Landau functionals

Traditionally, only the time-even channel of Skyrme functionals has been adjusted to selected experimental data. That is, the time-odd channel has usually not been constrained.
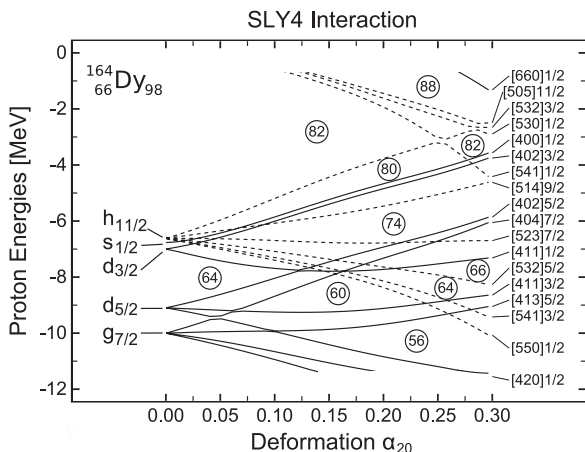
FIG. 4. Nilsson proton levels of SLy4 in ^{164}Dy as a function of the axial quadrupole deformation α_{20} ($\alpha_{22} = 0$).

This is illustrated by the broad spread of the values of the isoscalar Landau parameters g_0 and g_1 of the standard Skyrme functionals [23,72]. In Ref. [23], a careful study of Gamow-Teller resonances within the Skyrme EDF theory yielded a set of "optimal" Landau parameters that could be used to fix some of the coupling constants of the time-odd channel of the functional (namely, C_t^s and C_t^T).

As reported in Table III, the time-odd polarization in the Landau variant is greater than in the native variant, with the largest shift growing to 231 keV. The time-odd shifts in the gauge variant are generally smaller than for the native and Landau parametrizations. They also have opposite sign (time-odd polarization in the gauge variant decreases the binding energy, while it is repulsive in the native and Landau variants).

The black bins in Figs. 1–3 show ΔE^{Todd} for Landau-corrected functionals. The effect of this correction is significant, as it shifts the centroid of most histograms by about 100 keV for SIII and SkP and 50 keV for SLy4. When only ground states are considered, the overall shift is of the order of 50 keV.

To finish this section, let us recall that setting $C_1^{\Delta s} = 0$ was motivated in Ref. [23] to reproduce the energy and strength of the GT resonance, although different conclusions about the role of this term were obtained later, in Ref. [73]. In any case, the isoscalar channel governed by the $C_0^{\Delta s}$ term is not constrained by GT resonances, and in Refs. [6,13,23], and [72], and these terms are set to zero essentially to ensure the stability of the calculation. We briefly discuss this point in Sec. IV E.

3. Alignments and choice of the quantization axis

As discussed in Sec. II E, one of the characteristic features of the treatment of odd nuclei in the blocking approximation is the dependence of time-odd densities on the orientation of the alignment vector with respect to the principal axes or, equivalently, the choice of the self-consistent symmetries and quantization axis. To measure this effect, we performed two sets of calculations. The first variant ($\perp$) corresponds to the alignment vector aligned along the y axis and the shape symmetry axis aligned along the z axis. In the terminology of the cranking model, this case represents "collective rotation" perpendicular to the symmetry axis. In the second variant ($\parallel$), the nucleus is rotated by 90º, as described in Sec. III A, so that the alignment and symmetry axes coincide with the y axis ("noncollective rotation").

Note that in both situations the y signature and parity are conserved: the identification of blocking configurations via the position of the blocked state in a given signature/parity block hence provides a very robust way of tracking configurations before and after the Euler rotation, as it is independent of the changes in other *spatial* characteristics of the q.p. wave functions. As mentioned in Sec. III A, the original Nilsson label of a q.p. state can be easily recovered in the noncollective orientation by simply exchanging the roles of the z and y axes in their computation.

In Fig. 5 we show the distribution of differences, $\Delta E^j = E_{\text{qp}}^{\parallel} - E_{\text{qp}}^{\perp}$, for the 3822 cases presented in the previous section
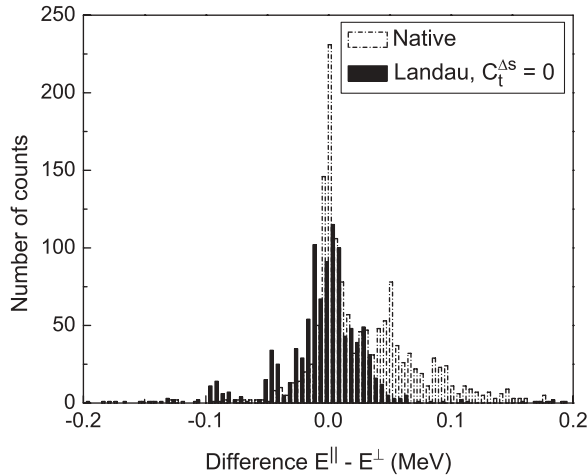
FIG. 5. Cumulative histogram of deviations $\Delta E^j = E^{\parallel}_{\mathrm{qp}} - E^{\perp}_{\mathrm{qp}}$ between energies of one-quasiproton states calculated in the noncollective-rotation ($\parallel$) and collective-rotation ($\perp$) variants. Dot-dashed open bins, native variants; filled bins, Landau variants. The bin size is 5 keV.

(only those well converged are included in the plot). It is shown that the time-odd polarization owing to the orientation of q.p. alignment gives an appreciable contribution to the time-odd shift, with the average value of ΔE^j being about 50 keV in the native variant. The orientation effect seems to be weaker for Landau functionals. While the energy shift ΔE^j depends on the actual configuration, the total energy in the collective rotation scenario ($\perp$) is overall lower than in the noncollective one ($\parallel$) when native functionals are used.

C. Experimental odd-proton spectra

In well-deformed nuclei, one-q.p. states can be related to the rotational band-head configurations [74]. In rare-earth nuclei, rich systematics of experimental data exist, and most importantly, the customary assignments of Nilsson labels $[Nn_z\Lambda]\Omega$ are available [30,75]. Although these labels are approximate, they facilitate the comparison between theory and experiment.

In Fig. 6 we show the one-quasiproton spectra for the Ho ($Z = 67$) isotopic chain predicted with SkP (upper-left panel), SIII (lower-left panel), and SLy4 (lower-right panel) functionals in the native variant. They are compared to experimental data. We follow the convention of Refs. [30] and [76], whereby the holelike excitations are plotted below zero (representing the ground-state configuration), while the particle-like states are plotted above zero.

The comparison with experiment suggests that the functional parametrizations employed in our work are not of spectroscopic quality for deformed nuclei. While the general deformation trends are reproduced and most of the orbitals found experimentally are indeed predicted to appear around the Fermi level, the quantitative agreement with the data is not particularly impressive. For example, the SLy4 parametrization fails to reproduce the observed [523]7/2 ground state of Ho isotopes; this state is predicted to lie 300–500 keV above the calculated [411]1/2 ground state. Surprisingly, the oldest Skyrme parametrization SIII gives the best reproduction of experimental band heads. The result in Fig. 6 is consistent with the conclusions in Ref. [38]; they found that the agreement of both spin and parity in the self-consistent models reaches about 40% for well-deformed nuclei regardless of the Skyrme force used.

The three functionals used here have different isoscalar effective masses; $m^* = 1$, 0.707, and 0.7 for SkP, SIII, and SLy4, respectively. The effect of m^* on shell structure is complex [7]; among others, it impacts the density of states around the Fermi level. As shown in Fig. 6, the average level density obtained with SkP is indeed close to the experimental one. However, this does not necessarily mean that the spectroscopic properties are better described with this
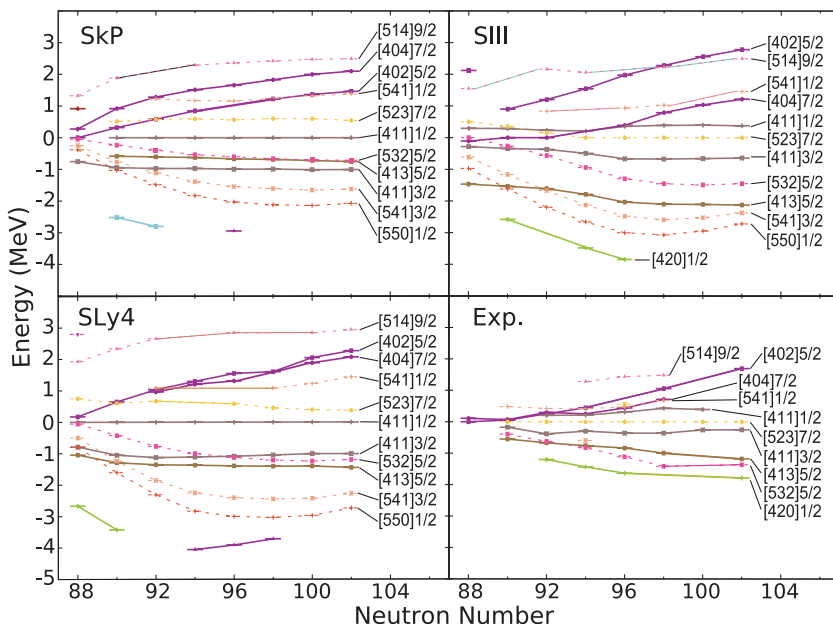

FIG. 6. (Color online) One-quasiproton band-head energies: calculated with SkP (top left), SIII (top right), and SLy4 (bottom left) Skyrme functionals, and extracted from experimental data (bottom right), plotted versus neutron number for Ho isotopes. Hole states are plotted below the ground state (zero energy) and particle states are plotted above. The time-odd terms are included in the native variant. Experimental data are taken from Refs. [30] and [75].

interaction: just as for SLy4, the ground state is incorrectly assigned to the [411]1/2 orbital for all isotopes.

There are, indeed, many factors that may impact the order of one-q.p. states. The recent analysis of spherical s.p. shell structure [7] has demonstrated that the isoscalar coupling constants in EDF have a large impact on the position of s.p. energies and spin-orbit splitting. It was also shown that the role of the effective-mass coupling constant cannot be reduced to merely changing the overall density of states. In fact, effective mass significantly influences relative positions of s.p. levels, including the splitting of spin-orbit partners.

D. Triaxial shape polarization

Triaxial deformations of nuclear shape are enhanced at high spins [77,78]. One spectacular example is the nuclear wobbling motion, which is caused by the fast rotation of triaxially deformed nuclei [74,79–81]. The phenomenon of nuclear chirality is also tightly related to axial asymmetry [54,82,83]. Recently, a systematic study of ground-state nuclear shapes in the framework of the macroscopic-microscopic model has also pointed to regions of triaxial instability in the nuclear chart [84].

In the deformed rare-earth region that we consider in this work, the blocking of a q.p. built on intruder configurations has a strong γ-driving effect [85–88]. Most of the studies of this phenomenon are so far confined to high-spin states. Our calculations offer the opportunity to assess the degree of triaxiality in the ground-state configurations associated with weakly spin-polarized states.

The calculated equilibrium deformations of one-quasiproton configurations considered in our survey are displayed in Fig. 7. Time-odd terms are set to zero, so that results can be compared with the time-even calculations performed with HFBTHO that define the axial reference point. As is apparent in Fig. 7, for the majority of configurations, triaxiality is very small, with γ deformation typically less than 1°.
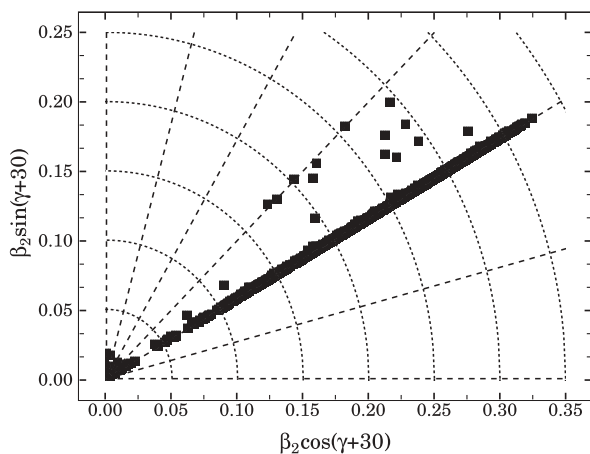

FIG. 7. Distribution of equilibrium deformations in the (X, Y) plane, $X = \beta \cos[\gamma + (\pi/6)]$ and $Y = \beta \sin[\gamma + (\pi/6)]$, where β and γ are the standard Bohr quadrupole deformation parameters. The figure corresponds to the 3822 different blocked configurations considered in this study. Time-odd terms are set to zero.

TABLE IV. Equilibrium deformation of the [402]3/2 blocked configuration in several odd-proton isotopes with the SLy4 interaction (time-odd terms set to zero). $\Delta^\gamma E$ represents the gain (keV) in energy induced by the triaxiality.

Z	N	E^* (MeV)	β	γ (deg)	$\Delta^\gamma E$ (keV)
69	90	1.506	0.21	7.7	−191
69	92	2.070	0.25	6.7	−187
69	94	2.471	0.28	5.9	−191
69	96	2.745	0.29	5.4	−184
69	98	2.955	0.30	4.0	−124
71	86	0.232	0.13	19.6	−233
71	88	0.647	0.17	11.8	−214
71	90	1.106	0.20	8.9	−195
73	88	0.442	0.16	8.1	−203
73	90	0.717	0.18	8.9	−205

Only a few highly excited states are characterized by a sizable triaxial polarization: one such example is the state [402]3/2, which originates from the spherical $d_{3/2}$ orbital from the $N = 4$ major shell and is pushed up into the $N = 5$ major shell because of deformation. In Table IV we report the equilibrium deformations calculated with SLy4 for this specific configuration in a number of isotopes. The excitation energies of [402]3/2 range from 0.2 to 3 MeV. On average, the net energy gain induced by the triaxial polarization of the core is of the order of 200 keV in this extreme case.

As indicated, the results presented in Fig. 7 were obtained by setting all time-odd fields to zero. When this constraint is released, ground-state configurations remain overwhelmingly axial, independently of the orientation of the alignment vector (cf. discussion in Sec. II E). However, we do observe that in the collective orientation limit, low-j intruder states, such as [541]1/2 (from $h_{9/2}$) and [550]1/2 (from $h_{11/2}$), or high-j intruder states, such as [505]11/2 (from $h_{11/2}$), seem slightly more unstable against γ polarization than in the noncollective situation.

This overall axial stability is illustrated in Fig. 8, where the distributions of the γ angles for well-deformed odd-proton states in the rare-earth nuclei are plotted. For better legibility of the figure, the very rare pronounced triaxial cases with $\gamma > 2°$ have been omitted; they have already been discussed, and so have the many near-axial states with $\gamma < 0.05°$. In the lower panel corresponding to the collective orientation, the few points beyond $\gamma = 1°$ correspond to the γ-driving orbitals. If the rotational frequency ω_y is increased (cranking), we find that the degree of triaxiality increases accordingly [85,87,89].

E. Finite-size instabilities of band-head calculations

It has been shown that some parametrizations of the Skyrme energy functional could be prone to finite-size instabilities [90–92]. In particular, the time-even $C_t^{\Delta\rho}\rho_t\Delta\rho_t$ and time-odd $C_t^{\Delta s}s_t\Delta s_t$ terms could, in some cases, lead to divergences of the HFB iterative procedure. The size of these instabilities depends on a number of factors, such as the EDF parametrization, particle number, and specific implementation of the DFT solver. The detailed analysis of EDF instabilities
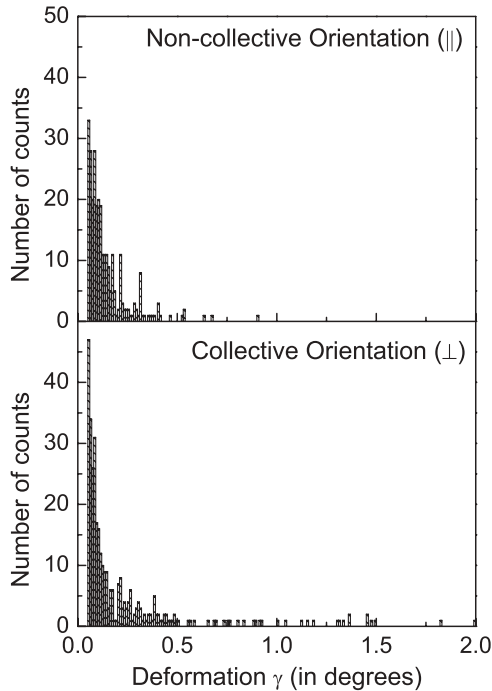
FIG. 8. Triaxiality (measured by the angle γ) of well-deformed odd-proton states ($\beta > 0.1$) in the rare-earth region calculated with SIII, SkP, and SLy4 EDFs for the two orientations discussed in Sec. IV B3: collective (top) and noncollective (bottom).

performed in Ref. [92] was based on the RPA response function approach of Ref. [93] applied to Skyrme functionals [94,95]. Results were reported in ^{40}Ca and ^{56}Ni for the SkP and SLy5 parametrizations.

Finite-size instabilities governed by $C_t^{\Delta s}$ terms are amplified in polarized systems such as odd-mass nuclei. Indeed, these terms are only active when time-reversal symmetry is broken. As shown in Sec. IV B, the impact of time-odd components is weak, at least in the rare-earth region that we study. It is therefore possible to scale these terms by slightly varying the values of $C_t^{\Delta s}$, without impacting the calculated properties significantly. By contrast, scaling the coupling constants $C_t^{\Delta \rho}$ could result in totally nonphysical solutions.

According to Ref. [92], the functionals employed in this work, namely, SIII, SkP, and SLy4, should not be particularly sensitive to spin instabilities. Indeed, the rate of convergence in our calculations is of the order of 40%–50% for those three cases. This is less than for even-even axially deformed nuclei, but this rate can be tied to factors such as collapse of pairing, level crossings, etc.

However, other Skyrme parametrizations may be prone to severe and systematic divergences. To illustrate this point, we have performed a set of calculations with three functionals: SkO [96], SkP, and SkM* [97]. For each of those, we have used the native variant of the time-odd terms; only $C_0^{\Delta s}$ is multiplied by a scaling factor α ranging between 0 (no coupling) and 1 (standard coupling). A measure of stability of the iterative process is the rate of convergence for a predefined set of one-q.p. states. A result is deemed converged if the binding energy
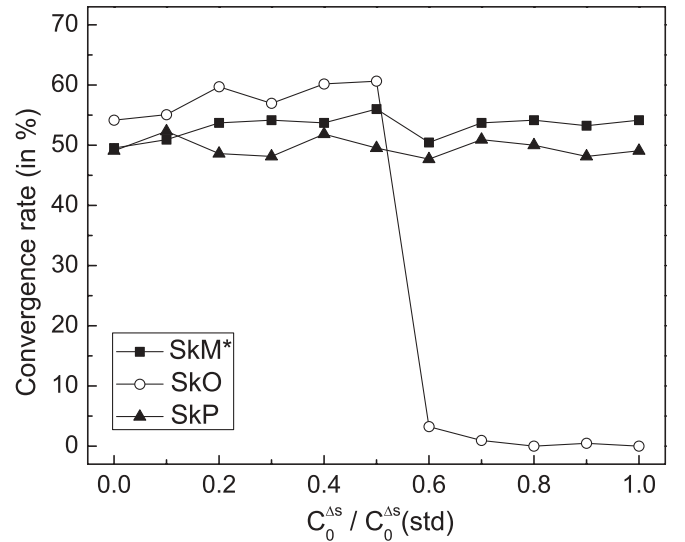

FIG. 9. Convergence rate of HFB equations with SkP, SkO, and SkM* functionals for one-quasiproton states in odd-A Ho isotopes with $88 \leqslant N \leqslant 104$ as a function of the scalar-isoscalar coupling constant $C_0^{\Delta s}$. See text for details.

does not change by more than 2 keV from one iteration to the next for three consecutive iterations. We show in Fig. 9 the evolution of this convergence rate as a function of α. Our set of configurations consists of 24 different one-quasiproton states in nine odd-A Ho isotopes with $88 \leqslant N \leqslant 104$. Therefore, the sample size used to define the convergence rate is 216.

According to Fig. 9, SkM* and SkP parametrizations are stable with respect to variations of $C_0^{\Delta s}$, but the SkO functional exhibits a sharp drop in the convergence rate when $\alpha > 0.5$, that is, $C_0^{\Delta s} \gtrsim 35$ MeV. Preliminary investigation of the RPA response function [98] suggests that instabilities could occur for transferred momenta q of the order of 2.2–2.5 fm^{-1} for this particular value of $C_0^{\Delta s}$. These results agree nicely with the original findings in Ref. [92] and emphasize the need to test EDFs against finite-size instabilities.

V. CONCLUSIONS

In this work, we have carried out a systematic theoretical survey of one-quasiproton states in deformed rare-earth nuclei. Our study is based on the symmetry-unconstrained Skyrme HFB framework that fully takes into account time-odd polarization effects.

We show that the EFA is equivalent to full blocking when the time-odd fields are set to zero. In this case, an arbitrary combination of time-reversed orbits can be used to define the blocked orbit, and this can be nicely quantified by introducing the notion of alispin. We emphasize the role of symmetries, in particular, nuclear alignment properties, in the exact treatment of the blocked state.

Our systematic survey indicates that, when native functionals are employed, the contributions from time-odd fields to the energy of the ground state and low-lying excited states is rather small, about 50 keV on average, with a variation of about 100–150 keV. Significant differences are found from

one interaction to another, although the effect remains small for the three interactions considered. Correcting the time-odd channel (Landau functionals) increases the contribution of the time-odd channel to the total energy by about 50%. For the functionals in the gauge variant, the time-odd effects are weak and opposite in sign.

By explicit calculations we have demonstrated that the choice of the alignment orientation with respect to the quantization axis does impact predicted time-odd polarization energies. The resulting energy shifts are appreciable in the scale of predicted time-odd displacements.

Standard parametrizations of the Skyrme interaction, such as SIII, SkP, and SLy4, give a qualitative, but not quantitative, description of experimental one-quasiproton spectra in the rare-earth region. We find that the triaxial shape polarization effects are generally small in the nuclei considered. Finally, we point to the sensitivity of DFT calculations for one-q.p. states to finite-size instabilities of the underlying EDF. A detailed investigation of this effect is currently under way.

The weak impact of the time-odd fields on spectroscopic properties implies that global studies with symmetry-restricted HFB solvers such as HFBTHO could be very useful for extracting information related to isovector properties, shell structure, and shapes. For this purpose, time-odd fields may be safely neglected.

[1] I. Zh. Petkov and M. V. Stoitsov, *Nuclear Density Functional Theory*. Oxford Studies in Physics, Vol. 14 (Clarendon Press, Oxford, 1991).

[2] M. Bender, P.-H. Heenen, and P.-G. Reinhard, Rev. Mod. Phys. **75**, 121 (2003).

[3] G. A. Lalazissis, P. Ring, and D. Vretenar (eds.), *Extended Density Functionals in Nuclear Structure Physics* (Springer Verlag, Berlin, 2004).

[4] M. V. Stoitsov, J. Dobaczewski, W. Nazarewicz, and P. Borycki, Int. J. Mass. Spectrom **251**, 243 (2006).

[5] G. F. Bertsch, B. Sabbey, and M. Uusnäkki, Phys. Rev. C **71**, 054311 (2005).

[6] M. Zalewski, J. Dobaczewski, W. Satuła, and T. R. Werner, Phys. Rev. C **77**, 024316 (2008).

[7] M. Kortelainen, J. Dobaczewski, K. Mizuyama, and J. Toivanen, Phys. Rev. C **77**, 064307 (2008).

[8] G. F. Bertsch, D. J. Dean, and W. Nazarewicz, SciDAC Review **6**(Winter), 42 (2007).

[9] J. W. Negele and D. Vautherin, Phys. Rev. C **5**, 1472 (1972).

[10] S. K. Bogner, R. J. Furnstahl, and L. Platter, Eur. Phys. J. A **39**, 219 (2009).

[11] B. G. Carlsson, J. Dobaczewski, and M. Kortelainen, Phys. Rev. C **78**, 044326 (2008).

[12] T. Lesinski, M. Bender, K. Bennaceur, T. Duguet, and J. Meyer, Phys. Rev. C **76**, 014312 (2007).

[13] W. Satuła, R. A. Wyss, and M. Zalewski, Phys. Rev. C **78**, 011302(R) (2008).

[14] W. Satuła, M. Zalewski, J. Dobaczewski, P. Olbratowski, M. Rafalski, T. R. Werner, and R. A. Wyss, Int. J. Mod. Phys. E **18**, 808 (2009).

[15] J. Margueron, S. Goriely, M. Grasso, G. Coló, and H. Sagawa, J. Phys. G **36**, 125103 (2009).

[16] S. Goriely, N. Chamel, and J. M. Pearson, Phys. Rev. Lett. **102**, 152503 (2009).

[17] Y. M. Engel, D. M. Brink, K. Goeke, S. J. Krieger, and D. Vautherin, Nucl. Phys. **A249**, 215 (1975).

[18] E. Perlińska, S. G. Rohoziński, J. Dobaczewski, and W. Nazarewicz, Phys. Rev. C **69**, 014316 (2004).

[19] U. Post, E. Wüst, and U. Mosel, Nucl. Phys. **A437**, 274 (1985).

[20] B.-Q. Chen, P.-H. Heenen, P. Bonche, M. S. Weiss, and H. Flocard, Phys. Rev. C **46**, R1582 (1992).

[21] J. Dobaczewski and J. Dudek, Phys. Rev. C **52**, 1827 (1995); **55**, 3177(E) (1997).

[22] A. V. Afanasjev and P. Ring, Phys. Rev. C **62**, 031302(R) (2000).

[23] M. Bender, J. Dobaczewski, J. Engel, and W. Nazarewicz, Phys. Rev. C **65**, 054322 (2002).

[24] K. Rutz, M. Bender, J. A. Maruhn, P.-G. Reinhard, and W. Greiner, Nucl. Phys. **A634**, 67 (1998).

[25] M. Baranger and M. Vénéroni, Ann. Phys. **114**, 123 (1978).

[26] J. Dobaczewski and J. Skalski, Nucl. Phys. **A369**, 123 (1981).

[27] J. A. Maruhn, P.-G. Reinhard, P. D. Stevenson, and M. R. Strayer, Phys. Rev. C **74**, 027601 (2006).

[28] N. Hinohara, T. Nakatsukasa, M. Matsuo, and K. Matsuyanagi, Prog. Theor. Phys. (Kyoto) **115**, 567 (2006).

[29] W. Ogle, S. Wahlborn, R. Piepenbring, and S. Fredriksson, Rev. Mod. Phys. **43**, 424 (1971).

[30] W. Nazarewicz, M. A. Riley, and J. D. Garrett, Nucl. Phys. **A512**, 61 (1990).

[31] S. Ćwiok and W. Nazarewicz, Nucl. Phys. **A529**, 95 (1991).

[32] S. Ćwiok, S. Hofmann, and W. Nazarewicz, Nucl. Phys. **A573**, 356 (1994).

[33] A. Parkhomenko and A. Sobiczewski, Acta Phys. Pol. B **36**, 3115 (2005).

[34] K. Rutz, M. Bender, P.-G. Reinhard, and J. Maruhn, Phys. Lett. **B468**, 1 (1999).

[35] S. Ćwiok, W. Nazarewicz, and P.-H. Heenen, Phys. Rev. Lett. **83**, 1108 (1999).

[36] A. V. Afanasjev, T. L. Khoo, S. Frauendorf, G. A. Lalazissis, and I. Ahmad, Phys. Rev. C **67**, 024309 (2003).

[37] A. V. Afanasjev and H. Abusara, Phys. Rev. C **81**, 014309 (2010).

[38] L. Bonneau, P. Quentin, and P. Möller, Phys. Rev. C **76**, 024320 (2007).

[39] J. R. Stone and P.-G. Reinhard, Prog. Part. Nucl. Phys. **58**, 587 (2007).

[40] A. Bulgac, Preprint FT-194-1980, Central Institute of Physics, Bucharest, 1980; arXiv:nucl-th/9907088.

[41] J. Dobaczewski, H. Flocard, and J. Treiner, Nucl. Phys. **A422**, 103 (1984).

[42] J. Dobaczewski, W. Nazarewicz, T. R. Werner, J.-F. Berger, C. R. Chinn, and J. Decharg'e, Phys. Rev. C **53**, 2809 (1996).

[43] J. P. Blaizot and G. Ripka, *Quantum Theory of Finite Systems* (MIT Press, Cambridge, MA, 1986).

[44] P. Ring and P. Schuck, *The Nuclear Many-Body Problem* (Springer Verlag, Berlin, 1980).

[45] B. Banerjee, P. Ring, and H. J. Mang, Nucl. Phys. **A221**, 564 (1974).

[46] A. Faessler, M. Płoszajczak, and K. W. Schmid, Prog. Part. Nucl. Phys. **5**, 79 (1980).

[47] G. Bertsch, J. Dobaczewski, W. Nazarewicz, and J. Pei, Phys. Rev. A **79**, 043602 (2009).

[48] S. Perez-Martin and L. M. Robledo, Phys. Rev. C **78**, 014304 (2008).

[49] P.-H. Heenen, P. Bonche, and H. Flocard, Nucl. Phys. **A588**, 490 (1995).

[50] J. Dobaczewski, W. Satuła, B. G. Carlsson, J. Engel, P. Olbratowski, P. Powałowski, M. Sadziak, J. Sarich, N. Schunck, A. Staszczak, M. V. Stoitsov, M. Zalewski, and H. Zduńczuk, Comput. Phys. Commun. **180**, 2361 (2009).

[51] S. Perez-Martin and L. M. Robledo, Phys. Rev. C **76**, 064314 (2007).

[52] P. Olbratowski, J. Dobaczewski, and J. Dudek, Phys. Rev. C **73**, 054308 (2006).

[53] D. A. Varshalovich, A. N. Moskalev, and V. K. Khersonskii, *Quantum Theory of Angular Momentum* (World Scientific, Singapore, 1988).

[54] P. Olbratowski, J. Dobaczewski, J. Dudek, and W. Płóciennik, Phys. Rev. Lett. **93**, 052501 (2004).

[55] J. Dobaczewski and J. Dudek, Comput. Phys. Commun. **102**, 166 (1997); **102**, 183 (1997); **131**, 164 (2000); J. Dobaczewski and P. Olbratowski, *ibid.* **158**, 158 (2004).

[56] M. Girod and B. Grammaticos, Phys. Rev. C **27**, 2317 (1983).

[57] M. V. Stoitsov, J. Dobaczewski, W. Nazarewicz, and P. Ring, Comput. Phys. Commun. **167**, 43 (2005).

[58] J. Dobaczewski and P. Olbratowski, Comput. Phys. Commun. **167**, 214 (2005).

[59] M. Stoitsov, J. Dobaczewski, and W. Nazarewicz, AIP Conf. Proc. **726**, 57 (2004).

[60] J. Dobaczewski and J. Dudek, Comput. Phys. Commun. **102**, 166 (1997); **102**, 183 (1997).

[61] M. Beiner, H. Flocard, N. Van Giai, and P. Quentin, Nucl. Phys. **A238**, 29 (1975).

[62] E. Chabanat, P. Bonche, P. Haensel, J. Meyer, and R. Schaeffer, Nucl. Phys. **A635**, 231 (1998).

[63] J. Dobaczewski, W. Nazarewicz, and M. V. Stoitsov, Eur. Phys. J. A **15**, 21 (2002).

[64] A. Bulgac and Y. Yu, Phys. Rev. Lett. **88**, 042504 (2002).

[65] P. J. Borycki, J. Dobaczewski, W. Nazarewicz, and M. V. Stoitsov, Phys. Rev. C **73**, 044319 (2006).

[66] G. F. Bertsch, C. A. Bertulani, W. Nazarewicz, N. Schunck, and M. V. Stoitsov, Phys. Rev. C **79**, 034306 (2009).

[67] T. Lesinski, T. Duguet, K. Bennaceur, and J. Meyer, Eur. Phys. J. A **40**, 121 (2009).

[68] D. D. Johnson, Phys. Rev. B **38**, 12807 (1988).

[69] A. Baran, A. Bulgac, M. M. Forbes, G. Hagen, W. Nazarewicz, N. Schunck, and M. V. Stoitsov, Phys. Rev. C **78**, 014318 (2008).

[70] T. Duguet, P. Bonche, P.-H. Heenen, and J. Meyer, Phys. Rev. C **65**, 014310 (2001).

[71] T. Duguet, P. Bonche, P.-H. Heenen, and J. Meyer, Phys. Rev. C **65**, 014311 (2001).

[72] H. Zduńczuk, W. Satuła, and R. A. Wyss, Phys. Rev. C **71**, 024305 (2005).

[73] S. Fracasso and G. Coló, Phys. Rev. C **76**, 044307 (2007).

[74] A. Bohr and B. R. Mottelson, *Nuclear Structure* (Benjamin, New York, 1975), Vol. II.

[75] Evaluated Nuclear Structure Data File.

[76] B. S. Nielsen and M. E. Bunker, Nucl. Phys. **A245**, 376 (1975).

[77] Z. Szymański, *Fast Nuclear Rotation* (Clarendon Press, Oxford, 1983).

[78] S. Frauendorf, Rev. Mod. Phys. **73**, 463 (2001).

[79] T. Shoji and Y. R. Shimizu, Prog. Theor. Phys. **121**, 319 (2009).

[80] S. W. Ødegård *et al.*, Phys. Rev. Lett. **86**, 5866 (2001).

[81] D. R. Jensen *et al.*, Phys. Rev. Lett. **89**, 142503 (2002).

[82] S. Frauendorf and J. Meng, Nucl. Phys. **A617**, 131 (1997).

[83] B. Qi, S. Q. Zhang, J. Meng, S. Y. Wang, and S. Frauendorf, arXiv:0812.4597 [nucl-th].

[84] P. Möller, R. Bengtsson, B. G. Carlsson, P. Olivius, and T. Ichikawa, Phys. Rev. Lett. **97**, 162502 (2006).

[85] S. Frauendorf and F. R. May, Phys. Lett. **B125**, 245 (1983).

[86] I. Hamamoto and B. Mottelson, Phys. Lett. **B127**, 281 (1983).

[87] S. Åberg, Nucl. Phys. **A520**, 35c (1990).

[88] M. Matev, A. V. Afanasjev, J. Dobaczewski, G. A. Lalazissis, and W. Nazarewicz, Phys. Rev. C **76**, 034304 (2007).

[89] I. Hamamoto and B. Mottelson, Phys. Lett. **B127**, 281 (1983).

[90] J. P. Blaizot, Phys. Lett. **B60**, 435 (1976).

[91] E. Caurier and B. Grammaticos, Phys. Lett. **B92**, 236 (1980).

[92] T. Lesinski, K. Bennaceur, T. Duguet, and J. Meyer, Phys. Rev. C **74**, 044315 (2006).

[93] A. L. Fetter and J. D. Walecka, *Quantum Theory of Many-Particle Systems* (McGraw-Hill, Boston, 1971).

[94] C. García-Recio, J. Navarro, N. Van Giai, and N. N. Salcedo, Ann. Phys. **214**, 293 (1992).

[95] J. Margueron, J. Navarro, and N. Van Giai, Phys. Rev. C **74**, 015805 (2006).

[96] P.-G. Reinhard, D. J. Dean, W. Nazarewicz, J. Dobaczewski, J. A. Maruhn, and M. R. Strayer, Phys. Rev. C **60**, 014316 (1999).

[97] J. Bartel, P. Quentin, M. Brack, C. Guet, and H. B. Håkansson, Nucl. Phys. **A386**, 79 (1982).

[98] T. Lesinski (private communication).